ACS OMEGA

Open Access

http://pubs.acs.org/journal/acsodf

Article

SKOV-3 Cell Aggregates on a Microfluidic Chip with a Thermoresponsive Hydrogel as a Culture Scaffold for DOX Assessment

Tianzhu Zhang,* Liuxin Yang, Zhengyang Wang, and Naizhen Zhou

Cite This: *ACS Omega* 2025, 10, 14972−14979

Read Online

ACCESS | Metrics & More | Article Recommendations | Supporting Information

ABSTRACT: Microfluidic chip technology is very popular in life sciences. Here, ovarian cancer SKOV-3 cell aggregates were formed using thermoresponsive poly(*N*-isopropylacrylamide-*co*-acrylic acid) (PNA) hydrogel as a culture scaffold on a microfluidic chip serving as an operating platform. A simple microfluidic chip was designed and fabricated as the three-dimensional (3D) cell culture microplatform. Different concentrations of doxorubicin (DOX) were fed to the obtained SKOV-3 cell aggregates on the chip via a pump. All characterization results indicated that this system could effectively perform 3D cell culture and drug evaluation to a certain extent. In addition, by grafting the RGD sequence, the biocompatibility of the PNA hydrogel was improved. On the one hand, the grafting of the RGD sequence into the hydrogel could significantly improve cell proliferation in this system; on the other hand, it led to an earlier appearance of DOX drug resistance. This versatile model in this study has the potential for further use in in vitro human ovarian cancer physiological models, drug discovery, and toxicology research.

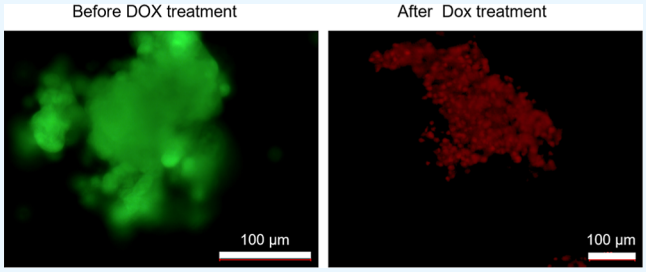

1. INTRODUCTION

Healthcare systems are faced with the challenge of providing access to innovative and lifesaving treatments while shouldering the cost of expensive medicines.[1] In a traditional way, high costs and the sacrifice of experimental animals pose significant obstacles. To address these issues, organ-on-a-chip technology has emerged as a promising solution. An organ-on-a-chip is a microfluidic platform that creates a controlled microenvironment with vasculature-like perfusion, integrating human multicellular structures to mimic the physiological architecture and function of human tissues and organs.[2,3]

Microfluidic chip technology is a chip-based operating platform that combines analytical chemistry and microelectromechanical system technology for studying life sciences.[4,5] Due to numerous unique advantages, such as small volume, controllable liquid flow, low consumption of sample reagents, and rapid analysis, it has become a research hotspot and key point in the fields of physics, chemistry, biology, medicine, and engineering.[6,7] The application purpose is to realize the ultimate goal of the microanalysis system—the chip lab, with the current work development primarily focused on the life science field.[8] Bionic lung, bionic liver, bionic kidney, bionic heart, bionic intestine, and other microfluidic chip models have been reported. These studies have academically demonstrated the feasibility of simulating the physiological structure of the human body on a thin slice with only several square centimeters in size, leading to the realization of the so-called organ chip.[9−11]

Three-dimensional (3D) cell culture technology has always played an important role in the field of tumor research.[12] Through using this 3D technology, diverse cell types can be cocultured in vitro on various carriers, which contribute to understanding the interactions between tumors and the stroma.[13,14] Hydrogels with good biocompatibility have been widely used in the in vitro cell culture.[15−17] Notably, environmentally sensitive hydrogels, especially thermo-responsive ones, are frequently used as a smart culture carrier.[18−23]

This work is based on a self-designed microfluidic chip serving as a platform to establish SKOV-3 spheroids for the DOX evaluation. The selected culture matrix was the thermoresponsive hydrogel PNIPAM,[24,25] which was further modified with RGD to improve biocompatibility based on our research.[26] The RGD sequence, composed of arginine, glycine, and aspartic acid, is present in a variety of extracellular matrices. It can specifically bind to integrin and effectively promote cell adhesion to biomaterials.[27,28] Through the aforementioned method, a tumor evaluation model was successfully established.

Received: November 13, 2024
Revised: January 25, 2025
Accepted: January 31, 2025
Published: April 9, 2025

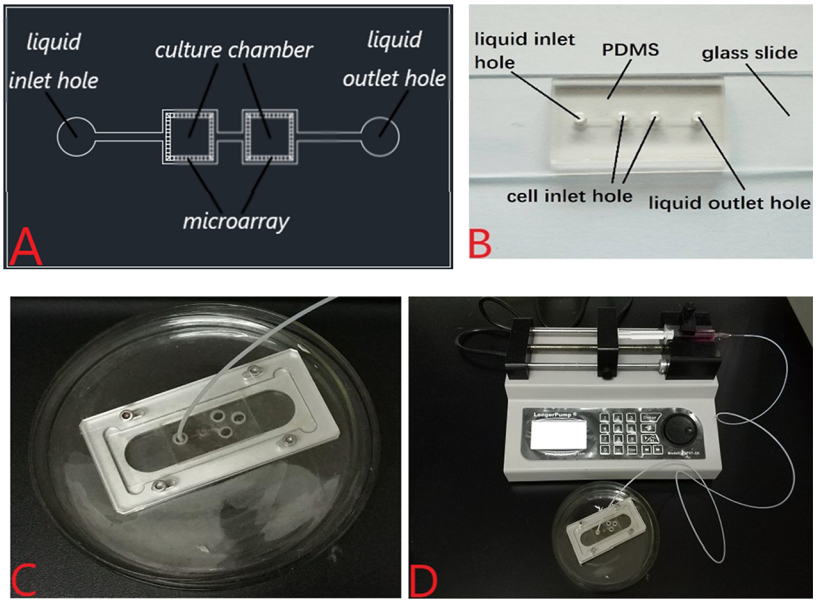

Figure 1. (A) Structural plan of the microfluidic chip; (B) physical product; (C) chip was clamped by a fixture; and (D) chip was equipped with a pump.

2. MATERIALS AND METHODS

2.1. Materials. *N*-Isopropylacrylamide (NIPAM), acrylic acid (AA), *N*,*N*′-methylenebis (acrylamide) (BIS), ammonium persulfate (APS), and sodium dodecyl sulfate (SDS) were purchased from Sinopharm Chemical Reagent Shanghai Co. Ltd. The c(RGDfK) was purchased from Bankpeptide Biological Technology Co. Ltd. (Hefei, China). Other biological reagents were purchased from KeyGEN BioTECH.

2.2. Microfluidic Device Fabrication. The microfluidic chip consisted of two cell culture chambers and is equipped with three injection pumps to control the liquid flow in the chips. As shown in Figure 1A, in the plan sketch of the microfluidic chip, there are two culture chambers (3000 × 3000 × 200 μm), one inlet hole (3 mm diameter), and one outlet hole (3 mm diameter).

Each culture chamber is wrapped by microarray columns with dimensions of 100 × 100 × 200 μm (a square in cross-section of 100 × 100 μm and a height of 200 μm) with a spacing of 8 μm between adjacent columns to ensure that the cells could remain in the culture chamber without being washed away. The microarray is surrounded by a liquid channel, with the main channel being 500 μm wide.

The entire chip was divided into two layers, as shown in Figure 1B. The upper layer was composed of PDMS and included various main structures such as liquid inlet hole, cell inlet holes, and liquid outlet hole. Cells were injected into the culture chamber through the cell inlet hole. Figure 1C,D shows the chip clamped by a fixture and equipped with a pump, respectively. There are compartments, one close to the inlet was used as control groups and another close to the outlet was used as the experiment group. In control groups, no drugs were loaded.

2.3. Preparation of PNA Hydrogels. PNA hydrogels were prepared according the reported method.[24,25] NIPAM (13.58 mmol), AA (0.14 mmol), BIS (0.28 mmol), and SDS (0.058 g, 2 mmol) were dissolved in 95 mL of water in a three-necked round-bottom flask equipped with a magnetic stir and heated to 70 °C under a gentle stream of nitrogen. After 1 h, APS (0.068 g, dissolved in 5 mL of water) was added to initiate the reaction. The reaction was allowed to proceed for 5 h. The resultant microgels were purified by dialysis (cut off 8000−15,000 Da) against water with regular water change (every day) for 1 week and then the obtained hydrogels were lyophilized for 48 h (Figure S1).

2.4. Graft of the RGD Sequence on Hydrogel. 0.0334 g of lyophilized hydrogels, 6×10^{-4} mol EDC·HCl, 6×10^{-4} mol NHS, and 10^{-5} mol RGD were dissolved in 100 mL of distilled water in a round flask. The system was stirred at room temperature for 48 h, and the pH was adjusted to 4.0−6.0. The grafted gels were purified by dialysis (cut off 8000−15,000 Da) against distilled water with frequent water changes (every 4 h) for at least 1 week and then the obtained hydrogels were lyophilized for 48 h (Figure S1). The RGD-grated hydrogel is named PNA-RGD.

2.5. Scanning Electron Microscopy Imaging. After swelling to equilibrium in double-distilled water at room temperature, the hydrogel samples were freeze-dried in a freeze drier (Song Yuan, LGJ-10, China) under vacuum at −42 °C for at least 48 h until all the solvent was sublimed. Subsequently, the freeze-dried hydrogels were carefully sectioned. The interior morphology of the hydrogel samples was examined by using a scanning electron microscope (ZEISS, Ultra Plus, Germany).

2.6. Rheology Measurement. The dynamic rheological behavior investigation of the hydrogels was carried out on an MCR302 rheometer (Anton Paar, Austria) equipped with a 25 mm diameter upper plate. After the excess water was gently eliminated, the swollen hydrogels were placed onto the center of the bottom plate of the testing machine. The viscoelastic properties of the hydrogels were determined by measuring changes in the storage modulus G' and the loss modulus G'' at 25 °C. The sample gap was set to be 1.0 mm. Frequency sweeps were performed at a frequency range of 0.1−100 rad/s and constant 0.1% shear strain in an oscillatory mode using the RheoCompass software.

2.7. X-ray Photoelectron Spectroscopy Measurements. The elemental composition of the hydrogel surfaces

https://doi.org/10.1021/acsomega.4c10301
ACS Omega 2025, 10, 14972−14979

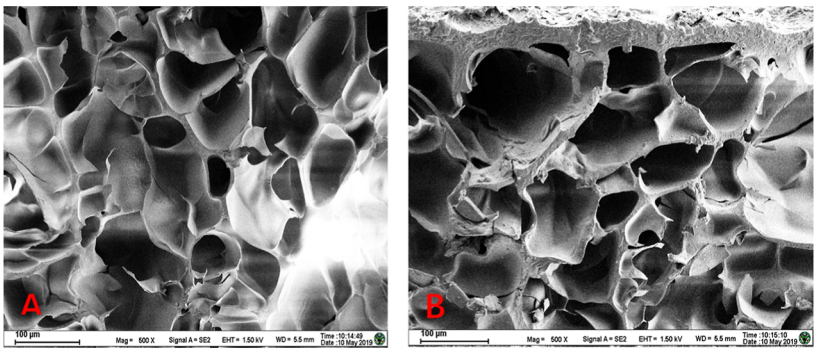

Figure 2. SEM picture of hydrogel PNA (A) and PNA-RGD (B).

was determined by X-ray photoelectron spectroscopy (XPS) (ESCALAB 250, Thermo Electron Corporation, USA). A monochromatic Al Kα X-ray source was operated at 1486.8 eV, and the anode X-ray source was operated at 15 kV. Survey spectra were acquired from 0 to 1200 eV binding energy. All spectra were collected at an electron takeoff angle of 45° from the surface under ultrahigh vacuum ($<10^{-8}$ torr). Binding energies relative to the C 1s peak (284.8 eV) were calibrated using hydrocarbons adsorbed on the surface of the samples. The high-resolution (pass energy = 20 eV) C 1s, O 1s and N 1s spectra were fitted and analyzed by XPSPEAK software.

2.8. Turbidity Measurements. The turbidity of the diluted microgel suspensions was measured on a TU-1810PC UV−vis spectrophotometer (Purkinje General, China) using water as a reference. The sample temperature was controlled with a refrigerated circulator.

2.9. Establishment of System. Two kinds of hydrogels, PNA and PNA-RGD, was dissolved with distilled water to obtain a 6 wt % aqueous suspension. The obtained suspensions were further mixed with an equal volume of SKOV-3 cells with a concentration of 5×10^5 cells/mL, respectively. Twenty microliters the mixture was added to each culture chamber of the microfluidic chip. The chip was placed in the incubator for about 2 h to ensure the sol was turned into a gel to encapsulate the cells. The medium was introduced into the culture chamber by a syringe pump and a capillary at a speed of 50 μL/h. The device was incubated at 37 °C in 5% CO_2 and 95% relative humidity. The morphological observation of multicellular mass was conducted by an inverted microscope (MF52) and photographed at 400× magnification using AxioVision Rel. 4.5 software. Morphology pictures of multicellular aggregates were taken on the first, third, fifth, and seventh days. Simultaneously, partial multicellular aggregates on the first, third, fifth, and seventh days were removed and placed in 96-well plates for further examination. Ten microliters of CCK-8 reagent was added to each well and incubated in the cell incubator for 2 h. The optical density (OD) was determined at the absorbance of 450 nm using a microplate reader (DeTie, HBS-1096A, China). The OD value is directly proportional to the number of living cells in the culture. Triplicates were performed for each group.

2.10. Assessment of Drug Sensitivity. After 4 d of cultivation, the cellular viability was the highest,[26] the drug DOX with different concentrations (μg/mL) (0, 0.25, 0.50, 1.00, 2.00, and 5.00) was introduced. After the cells were incubated for 24 h, partial multicellular aggregates were taken out and placed in 96-well plates. Then, 85 μL of 1 × Buffer A, 5 μL of PI dye, and 10 μL of FDA dye were injected into the well. The morphology of cellular aggregates was observed under a microscope (MShot, MF52, China).

Besides, the cell viability was also measured by the CCK-8 method. Ten microliters of CCK-8 reagent was added to each well, and then, these culture boards were incubated in the cell incubator for 2 h.

The control group was used as a reference without drug treatment. The cell viability was calculated by using the following equations

$$\text{cell viability} = \frac{\text{OD}_{\text{experiment}}}{\text{OD}_{\text{control}}} \times 100\% \quad (1)$$

where, the $\text{OD}_{\text{experiment}}$ is the OD of the experimental group and $\text{OD}_{\text{control}}$ is the OD of the control.

After treatment with DOX, a CCK-8 assay was conducted to determine its cytotoxicity. The cell survival rate was calculated using the following equation

$$\text{cell survival rate} = \frac{\text{OD}_1 - \text{OD}_0}{\text{OD}_2 - \text{OD}_{0'}} \quad (2)$$

where OD_1 is the absorbance of the experimental group, OD_2 is the absorbance of the untreated control, and OD_0 and $\text{OD}_{0'}$ are the background absorbance of the experimental group and the untreated control, respectively.

2.11. Statistical Analysis. All values were expressed as the mean ± the standard deviation, and at least three independent repeated experiments were conducted.

3. RESULTS AND DISCUSSION

3.1. Influence of RGD Grafting on Physical Properties of Hydrogel. According to the observations from SEM morphologies, thermoresponsiveness, and rheological behavior

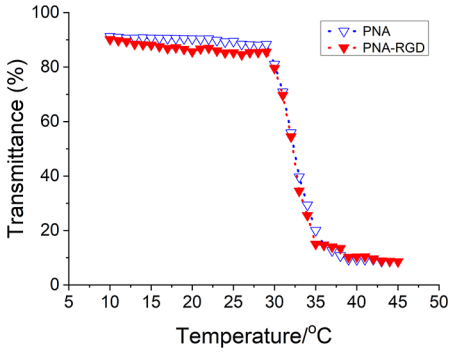

Figure 3. Thermoresponsivity of PNA and PNA-RGD hydrogel.

https://doi.org/10.1021/acsomega.4c10301
ACS Omega 2025, 10, 14972−14979

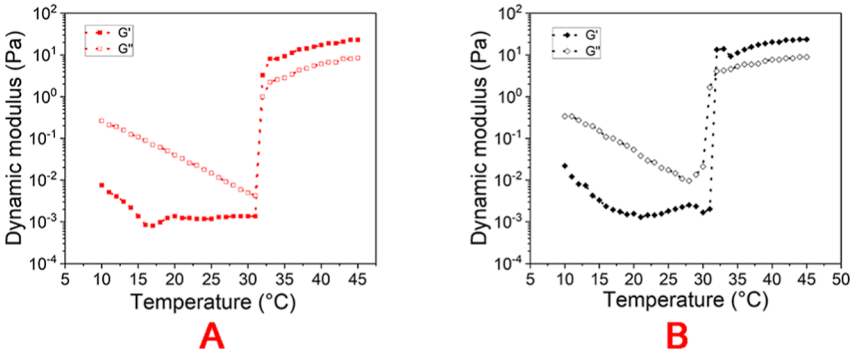

Figure 4. Change of modulus G' and G'' of hydrogels PNA (A) and PNA-RGD (B) with the temperature.

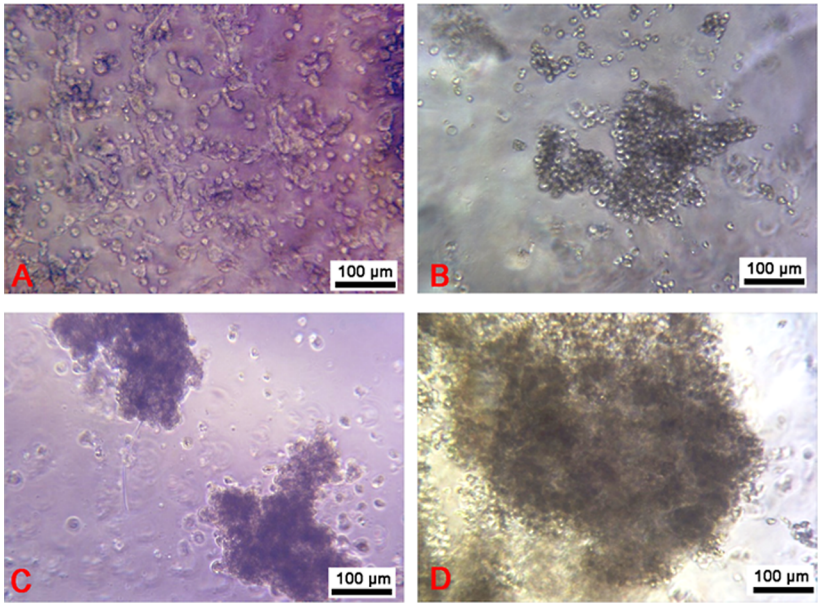

Figure 5. Morphological changes of SKOV-3 cell aggregates cultured in PNA hydrogels in a microfluidic chip (×100). (A) 1 d; (B) 3 d; (C) 5 d; and (D) 7 d.

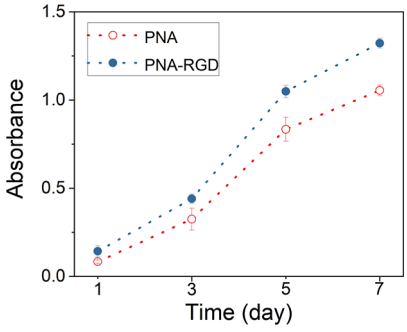

Figure 6. SKOV-3 cell proliferation curves in two hydrogels PNA and PNA-RGD (450 nm).

before and after RGD grafting (Figures 2−4), no significant change in the physical properties of the hydrogel was noted. This indicates that the grafting of RGD on PNA solely enhances the cyto-compatibility of the PNA hydrogel. As shown in Figure 3, the phase transition point of the PNA microgel is around 32 °C, in accordance with that reported in the literature.[23,29] According to a previous literature,[25] the hydrated particle size of PNA microgel particles changes from 85 nm at room temperature to around 40 nm at 37 °C. Due to the lower RGD grafting content, no characteristics of RGD can be observed in the XPS spectra (Figure S2).

3.2. Morphological Features of 3D Culture Model in Chip. The SKOV-3 cells were clustered in the PNA and PNA-RGD hydrogels. Figure 5 shows the change in cellular morphologies in the PNA hydrogel over time. On the first day, SKOV-3 cells were scattered in the field of vision and, on the third day, the cells had already formed aggregates in the hydrogel. The published literature showed that SKOV-3 cells formed cell spheres after 5 days of culture.[14] The volume of the cell aggregates gradually increased over time. Morphological observations indicated that SKOV-3 cells could cluster in hydrogels on the microfluidic chip. Similar phenomena in the PNA-RGD hydrogel also were observed. The proliferation curve of SKOV-3 cells cultured on PNA and PNA-RGD in the microfluidic chip is shown in Figure 6, indicating that PNA-RGD showed better cyto-compatibility than PNA. It could be seen from the curve that the period from the third to the fifth day was the exponential phase of cell proliferation, so the fifth day was selected as the time point of drug administration in the drug sensitivity test stage.

The main advantage of the chip platform is its ability to ensure a continuous supply of nutrients and convenient removal of metabolites through the flow. These conditions

https://doi.org/10.1021/acsomega.4c10301
ACS Omega 2025, 10, 14972−14979

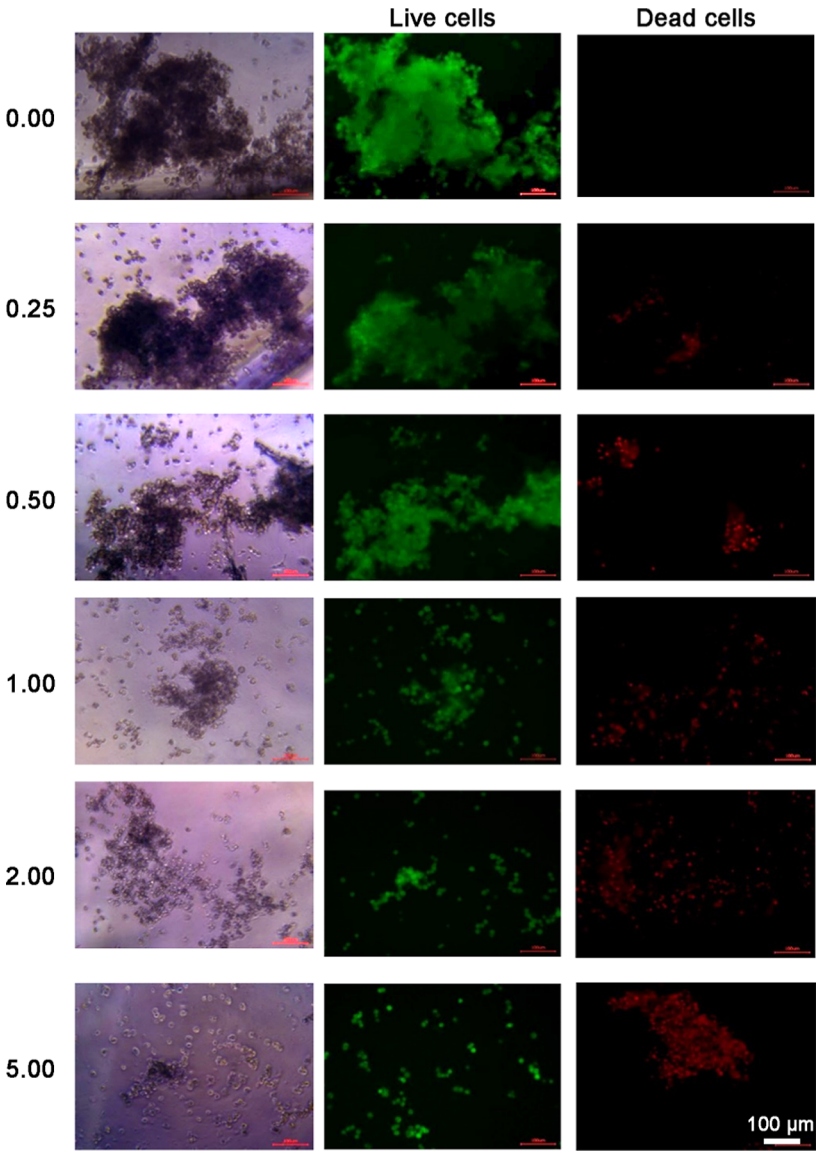

Figure 7. Effects of the different DOX concentrations on SKOV-3 cells in PNA hydrogels after 48 h by FDA/PI double staining (×100). The DOX concentration (μg/mL) in each group (from the top line to down line) was 0.00, 0.25, 0.50, 1.00, 2.00, and 5.00, respectively.

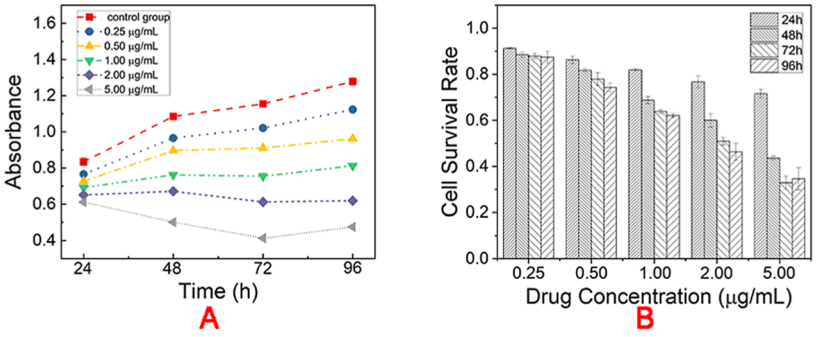

Figure 8. Absorbance curves (A) and cell survival rate (B) of SKOV-3 cells cultured in PNA treated with different concentrations of drug at different time points.

facilitate the growth and proliferation of the cancer cells. On the chip platform, after 7 days, SKOV-3 cell aggregates with a size of approximately 200 μm were formed. Under traditional culture conditions, where the culture medium was replaced halfway once per day, the proliferation of cells was much lower compared to that on the chip platform. In our other work,[26] SKOV-3 cell aggregates failed to form in a 96-well plate after 7 d, even though the culture medium was replaced halfway daily. The matrix used is RGD-grafted poly(ethylene glycol) (PEG)-cross-linked poly(methyl vinyl ether-*alt*-maleic acid) (P(MVE-

https://doi.org/10.1021/acsomega.4c10301
ACS Omega 2025, 10, 14972−14979

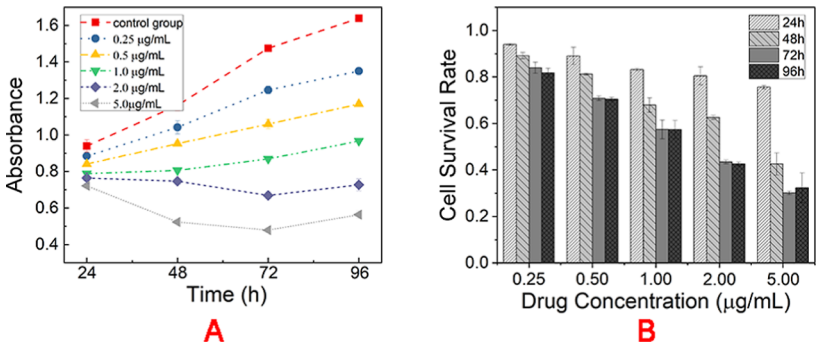

Figure 9. Absorbance curves (A) and survival rate (B) of SKOV-3 cells cultured in PNA-RGD treated with different concentrations of drugs at different time points.

alt-MA)) hydrogels (RGD-containing PEMM), which are similar to the PNA hydrogel. In the absence of RGD, another type of cancer cell, HepG2, exhibited a notably slower proliferation. HepG2 spheroids can only form after 7 days, reaching a size of less than 100 μm.[25]

3.3. Assessment of Drug Sensitivity. *3.3.1. Assessment of Drug Sensitivity in PNA.* After 48 h of drug treatment with different concentrations, FDA/PI double staining were performed, and the results are shown in Figure 7. The volume of the cell aggregates gradually decreased with an increase in the drug concentration. The gradual narrowing of the green area indicated that the number of living cells decreased with an increase in the drug concentration. The presence of a large amount of red fluorescence in cells treated with high concentrations (5 μg/mL) of the drug indicated cell death. However, SKOV-3 live cells observed under high drug concentration conditions may be apoptotic cells. Drug evaluation could be performed on the designed microfluidic chip according to the FDA/PI double staining results.

The absorbance values of SKOV-3 cells treated with different concentrations of DOX for 24, 48, 72, and 96 h, respectively, are depicted in Figure 8A. The absorbance values at 24 h with concentrations of 0.25, 0.5, and 1.0 μg/mL range from 0.77 to 0.61, which are close to the control group value, indicating that the drugs did not have a significant effect initially. From 48th h, the absorbance value at the same time point decreased with the increase in the drug concentration. Namely, the higher the DOX concentration, the lower the cell survival rate, as shown in Figure 8B. The lower DOX concentration, 0.25 μg/mL, did not notably inhibit cell proliferation; within 96 h, the SKOV3 cells still proliferated with the DOX treatment.

However, when the concentration of DOX increased to 0.5 μg/mL, the absorbance intensity increased from only 0.90 at 48th h to 0.91 at 72nd h. For the higher DOX concentration, as shown in Figure 8B, the cell survival rate decreased rapidly between 24 and 48 h after drug administration, especially in the experimental group with a concentration of 5.0 μg/mL. However, 5.0 μg/mL did not represent the most optimal concentration to inhibit the growth of cancer cells because it could be seen from Figure 8A that the cell viability of the 5.0 μg/mL experimental group had increased after 72 h, which means that the drug leads to a strong drug resistance with long-term use. Furthermore, it can be seen from Figure 8B that drug resistance is more obvious after treatment with large doses of drugs. After 96 h of 5.0 μg/mL DOX treatment, the cell survival rate inversely increased compared to that at 72 h. The emergence of drug resistance may be the adaptive changes that occur after cancer cells are exposed to fixed doses of drugs for a prolonged period.

3.3.2. Assessment of Drug Sensitivity in PNA-RGD. The RGD sequence consists of arginine, glycine, and aspartic acid and exists in a variety of extracellular matrices to promote cell adhesion to biological materials effectively. Here, the RGD sequence was grafted onto the PNA hydrogel to increase its biocompatibility. Figure 6 shows the proliferation of SKOV-3 cells in two kinds of hydrogels. It was clearly observed that the proliferation of cells in the PNA-RGD hydrogel was better than in the PNA hydrogel, which clearly indicates the function of RGD in the PNA hydrogel. Comparison of the average absorbance values at four time points revealed that the absorbance values in PNA-RGD, 0.143, 0.440, 1.049, and 1.323, were higher, respectively, than 0.083, 0.325, 0.834, and 1.055 in PNA. This demonstrates that the grafting of the RGD sequence into the hydrogel was successful and effective. The cell growth in PNA and PNA-RGD hydrogels under treatment with DOX at the same concentration is compared, as shown in Figure 9. The control group in Figure 9A has an absorbance value of 1.640 at 96th h, far exceeding the corresponding value in Figure 8A.

Different from the case in the PNA hydrogel, a higher concentration of DOX is required to significantly inhibit the proliferation of SKOV3 cells in PNA-RGD. As shown in Figure 9A, the DOX concentration is 2.0 μg/mL which can lead to the decrease in absorbance from 48th h in PNA-RGD hydrogel, whereas this concentration is only 1.0 μg/mL in the PNA hydrogel. In the absence of the RGD sequence, doxorubicin had a significantly higher inhibitory effect on cells between 48 and 72 h after treatment, while the drug inhibitory effect was significantly lower than that between 48th and 72nd h of drug treatment after the addition of the RGD sequence. The cells developed drug resistance to doxorubicin after 48 h of administration due to the presence of RGD sequence. Conversely, drug resistance in SKOV-3 cells raised lightly earlier in the PNA hydrogel than in the PNA-RGD hydrogel. The time is 72 h for 0.5 μg/mL drug treatment in the PNA hydrogel, while this time is 48 h in the PNA-RGD hydrogel for 1.0 μg/mL drug treatment, as clearly shown in Figure 9B. In fact, at 72 and 96 h, the cell survival rates are almost the same for 0.5 μg/mL drug. Our previous research results suggest that the binding of the SKOV-3 cells to the RGD on the hydrogel surface is initially involved in cell adhesion and spreading, which subsequently affected the expression of cancer cell stemness and EMT, leading to consequent drug resistance.[26]

https://doi.org/10.1021/acsomega.4c10301
ACS Omega 2025, 10, 14972−14979

4. CONCLUSIONS

In summary, in this study, SKOV-3 aggregates for drug evaluation were successfully established on microfluidic chips combined with a temperature-sensitive PNA hydrogel as a three-dimensional culture matrix. On the one hand, the grafting of the RGD sequence to the backbone of PNA remarkably improved the cytocompatibility of the hydrogels, thereby further enhancing the feasibility of this model. On the other hand, the presence of the RGD sequence in PNA-RGD significantly affected SKOV-3 cells' drug resistance to DOX. Specifically, SKOV-3 cells exhibited drug resistance earlier, and the same cell survival rate required a higher drug concentration when compared to the cell growth situation in both PNA and PNA-RGD after treatment with DOX at different concentrations. Overall, this model is versatile and demonstrates attractive potential applications in anticancer drug evaluation.

■ ASSOCIATED CONTENT

Supporting Information

The Supporting Information is available free of charge at https://pubs.acs.org/doi/10.1021/acsomega.4c10301.

Optical picture of PNA and PNA-RGD hydrogels and XPS N 1s spectra of PNA and PNA-RGD (PDF)

■ AUTHOR INFORMATION

Corresponding Author

Tianzhu Zhang − *State Key Laboratory of Digital Medical Engineering, School of Biological Science and Medical Engineering, Southeast University, Nanjing 210096, China;* orcid.org/0000-0002-4439-4334; Email: zhangtianzhu@seu.edu.cn

Authors

Liuxin Yang − *State Key Laboratory of Digital Medical Engineering, School of Biological Science and Medical Engineering, Southeast University, Nanjing 210096, China*

Zhengyang Wang − *State Key Laboratory of Digital Medical Engineering, School of Biological Science and Medical Engineering, Southeast University, Nanjing 210096, China*

Naizhen Zhou − *State Key Laboratory of Digital Medical Engineering, School of Biological Science and Medical Engineering, Southeast University, Nanjing 210096, China*

Complete contact information is available at: https://pubs.acs.org/10.1021/acsomega.4c10301

Notes

The authors declare no competing financial interest.

■ ACKNOWLEDGMENTS

The work was supported by Jiangsu Science and Technology Plan Project (BE2022741) and Suzhou Science and Technology Plan Project (SYG202343). The authors are also grateful for the generous technical supports from Prof. Zhang Yongjun of Nankai University.

■ REFERENCES

(1) Franzen, N.; van Harten, W. H.; Retèl, V. P.; Loskill, P.; van den Eijnden-van Raaij, J.; Ijzerman, M. Impact of organ-on-a-chip technology on pharmaceutical R&D costs. *Drug Discovery Today* **2019**, *24* (9), 1720−1724.

(2) Sun, L.; Chen, H.; Xu, D.; Liu, R.; Zhao, Y. Developing organs-on-chips for biomedical applications. *Smart Medicine* **2024**, *3* (2), No. e20240009.

(3) Shoji, J. Y.; Davis, R. P.; Mummery, C. L.; Krauss, S. Global literature analysis of organoid and organ-on-chip research. *Adv. Healthcare Mater.* **2024**, *13* (21), No. e2301067.

(4) Özkale, B.; Lou, J.; Ozelci, E.; Elosegui-Artola, A.; Tringides, C. M.; Mao, A. S.; Sakar, M. S.; Mooney, D. J. Actuated 3D microgels for single cell mechanobiology. *Lab Chip* **2022**, *22* (10), 1962−1970.

(5) Özkale, B.; Parreira, R.; Bekdemir, A.; Pancaldi, L.; Özelçi, E.; Amadio, C.; Kaynak, M.; Stellacci, F.; Mooney, D. J.; Sakar, M. S. Modular soft robotic microdevices for dexterous biomanipulation. *Lab Chip* **2019**, *19* (5), 778−788.

(6) Maschmeyer, I.; Lorenz, A. K.; Schimek, K.; Hasenberg, T.; Ramme, A. P.; Hubner, J.; Lindner, M.; Drewell, C.; Bauer, S.; Thomas, A.; et al. A four-organ-chip for interconnected long-term co-culture of human intestine, liver, skin and kidney equivalents. *Lab Chip* **2015**, *15* (12), 2688−2699.

(7) Moshksayan, K.; Kashaninejad, N.; Warkiani, M. E.; Lock, J. G.; Moghadas, H.; Firoozabadi, B.; Saidi, M. S.; Nguyen, N.-T. Spheroids-on-a-chip: Recent advances and design considerations in microfluidic platforms for spheroid formation and culture. *Sens. Actuators, B* **2018**, *263*, 151−176.

(8) Marsano, A.; Conficconi, C.; Lemme, M.; Occhetta, P.; Gaudiello, E.; Votta, E.; Cerino, G.; Redaelli, A.; Rasponi, M. Beating heart on a chip: a novel microfluidic platform to generate functional 3D cardiac microtissues. *Lab Chip* **2016**, *16* (3), 599−610.

(9) Hwan Sung, J. From organ-on-a-chip towards body-on-a-chip. *Biocell* **2022**, *46* (5), 1177−1180.

(10) Singh, D.; Mathur, A.; Arora, S.; Roy, S.; Mahindroo, N. Journey of organ on a chip technology and its role in future healthcare scenario. *Appl. Surf. Sci. Adv.* **2022**, *9*, 100246.

(11) Du, Y.; Li, N.; Yang, H.; Luo, C.; Gong, Y.; Tong, C.; Gao, Y.; Lu, S.; Long, M. Mimicking liver sinusoidal structures and functions using a 3D-configured microfluidic chip. *Lab Chip* **2017**, *17* (5), 782−794.

(12) Rodrigues, J.; Heinrich, M. A.; Teixeira, L. M.; Prakash, J. 3D *in vitro* model (r)evolution: unveiling tumor-stroma interactions. *Trends in Cancer* **2021**, *7* (3), 249−264.

(13) Williams, N. P.; Rhodehamel, M.; Yan, C.; Smith, A. S. T.; Jiao, A.; Murry, C. E.; Scatena, M.; Kim, D. H. Engineering anisotropic 3D tubular tissues with flexible thermoresponsive nanofabricated substrates. *Biomaterials* **2020**, *240*, 119856.

(14) Zhou, N.; Ma, X.; Bernaerts, K. V.; Ren, P.; Hu, W.; Zhang, T. Expansion of ovarian cancer stem-like cells in poly(ethylene glycol)-cross-linked poly(methyl vinyl ether-*alt*-maleic acid) and alginate double-network hydrogels. *ACS Biomater. Sci. Eng.* **2020**, *6* (6), 3310−3326.

(15) Nicolas, J.; Magli, S.; Rabbachin, L.; Sampaolesi, S.; Nicotra, F.; Russo, L. 3D extracellular matrix mimics: fundamental concepts and role of materials chemistry to influence stem cell fate. *Biomacromolecules* **2020**, *21* (6), 1968−1994.

(16) Safi, C.; Solano, A. G.; Liberelle, B.; Therriault, H.; Delattre, L.; Abdelkhalek, M.; Wang, C.; Bergeron-Fortier, S.; Moreau, V.; De Crescenzo, G.; et al. Effect of chitosan on alginate-based macroporous hydrogels for the capture of glioblastoma cancer cells. *ACS Appl. Bio Mater.* **2022**, *5* (9), 4531−4540.

(17) Bouhlel, W.; Kui, J.; Bibette, J.; Bremond, N. Encapsulation of cells in a collagen matrix surrounded by an alginate hydrogel shell for 3D cell culture. *ACS Biomater. Sci. Eng.* **2022**, *8* (6), 2700−2708.

(18) Tam, R. Y.; Smith, L. J.; Shoichet, M. S. Engineering cellular microenvironments with photo- and enzymatically responsive hydrogels: toward biomimetic 3D cell culture models. *Acc. Chem. Res.* **2017**, *50* (4), 703−713.

(19) Li, S.; Wang, W.; Li, W.; Xie, M.; Deng, C.; Sun, X.; Wang, C.; Liu, Y.; Shi, G.; Xu, Y.; et al. Fabrication of thermoresponsive hydrogel scaffolds with engineered microscale vasculatures. *Adv. Funct. Mater.* **2021**, *31* (27), 2102685.

(20) Lee, E. A.; Kim, S.; Jin, Y.; Cho, S. W.; Yang, K.; Hwang, N. S.; Kim, H. D. *In situ* microenvironment remodeling using a dual-responsive system: photodegradable hydrogels and gene activation by visible light. *Biomater. Sci.* **2022**, *10* (14), 3981−3992.
(21) Ma, P.; Lai, X.; Luo, Z.; Chen, Y.; Loh, X. J.; Ye, E.; Li, Z.; Wu, C.; Wu, Y. L. Recent advances in mechanical force-responsive drug delivery systems. *Nanoscale Adv.* **2022**, *4* (17), 3462−3478.
(22) Ekerdt, B. L.; Fuentes, C. M.; Lei, Y.; Adil, M. M.; Ramasubramanian, A.; Segalman, R. A.; Schaffer, D. V. Thermoreversible hyaluronic acid-PNIPAAm. hydrogel systems for 3D stem cell culture. *Adv. Healthcare Mater.* **2018**, *7* (12), No. e1800225.
(23) Yang, L.; Ren, P.; Wei, D.; Liang, M.; Xu, L.; Tao, Y.; Jiao, G.; Zhang, T.; Zhang, Q. Temperature-controlled screening of catechol groups in poly(*n*-isopropylacrylamide-co-dopamine methacrylamide) for cell detachment. *ACS Appl. Polym. Mater.* **2024**, *6* (4), 2061−2075.
(24) Gan, T.; Guan, Y.; Zhang, Y. Thermogelable PNIPAM microgel dispersion as 3D cell scaffold: effect of syneresis. *J. Mater. Chem. C* **2010**, *20* (28), 5937−5944.
(25) Wang, D.; Cheng, D.; Guan, Y.; Zhang, Y. Thermoreversible hydrogel for in situ generation and release of HepG2 spheroids. *Biomacromolecules* **2011**, *12* (3), 578−584.
(26) Zhou, N.; Ma, X.; Hu, W.; Ren, P.; Zhao, Y.; Zhang, T. Effect of RGD content in poly(ethylene glycol)-crosslinked poly(methyl vinyl ether-*alt*-maleic acid) hydrogels on the expansion of ovarian cancer stem-like cells. *Mater. Sci. Eng. C* **2021**, *118*, 111477.
(27) Oyama, E.; Takahashi, H.; Ishii, K. Effect of amino acids near the RGD sequence on binding activities between alphaIIbbeta3 integrin and fibrinogen in the presence of RGD-containing synthetic peptides from elegantin and angustatin. *Peptides* **2017**, *96*, 31−37.
(28) Dumbleton, J.; Shamul, J. G.; Jiang, B.; Agarwal, P.; Huang, H.; Jia, X.; He, X. Oxidation and RGD modification affect the early neural differentiation of murine embryonic stem cells cultured in core-shell alginate hydrogel microcapsules. *Cells Tissues Organs* **2022**, *211* (3), 294−303.
(29) Li, X.-H.; Liu, C.; Feng, S.-P.; Fang, N. X. Broadband light management with thermochromic hydrogel microparticles for smart windows. *Joule* **2019**, *3* (1), 290−302.

https://doi.org/10.1021/acsomega.4c10301
ACS Omega 2025, 10, 14972−14979